Full Paper
doi.org/10.1002/chem.201905759

Actinides | *Hot Paper*

Mononuclear to Polynuclear U^{IV} Structural Units: Effects of Reaction Conditions on U-Furoate Phase Formation

Nicole A. Vanagas,[a] Robert F. Higgins,[b] Jennifer N. Wacker,[a, d] Dane Romar C. Asuigui,[a] Evan Warzecha,[c] Stosh A. Kozimor,[d] Sarah L. Stoll,[a] Eric J. Schelter,[b] Jeffery A. Bertke,[a] and Karah E. Knope*[a]

Abstract: Uranium(IV) complexation by 2-furoic acid (2-FA) was examined to better understand the effects of ligand identity and reaction conditions on species formation and stability. Five compounds were isolated: $[UCl_2(2\text{-}FA)_2(H_2O)_2]_n$ (**1**), $[U_4Cl_{10}O_2(THF)_6(2\text{-}FA)_2]\cdot 2\,THF$ (**2**), $[U_6O_4(OH)_4(H_2O)_3(2\text{-}FA)_{12}]\cdot 7\,THF\cdot H_2O$ (**3**), $[U_6O_4(OH)_4(H_2O)_2(2\text{-}FA)_{12}]\cdot 8.76\,H_2O$ (**4**), and $[U_{38}Cl_{42}O_{54}(OH)_2(H_2O)_{20}]\cdot m\,H_2O\cdot n\,THF$ (**5**). The structures were determined by single-crystal X-ray diffraction and further characterized by Raman, IR, and optical absorption spectroscopy. The thermal stability and magnetic behavior of the compounds were also examined. Variations in the synthetic conditions led to notable differences in the structural units observed in the solid state. At low H_2O/THF ratios, a tetranuclear oxo-bridged $[U_4O_2]$ core was isolated. Aging of this solution resulted in the formation a U_{38} oxo cluster capped by chloro and water ligands. However, at increasing water concentrations only hexanuclear units were observed. In all cases, at temperatures of 100–120 °C, UO_2 nanoparticles formed.

Introduction

Hydrolysis and condensation are common to most metal ions on the periodic table.[1] For the actinides, in particular, such reactions are known to complicate their solution behavior and pose significant challenges in our ability to predict the fate of these elements under a range of technologically, scientifically, and environmentally relevant conditions.[2] Indeed, recognition of the importance of these reactions to our understanding of actinide chemical behavior has fueled recent work focused on the solution and solid-state structural characterization of polynuclear actinide structural units.[3] One of the principle factors governing the extent to which such reactions occur is the valence of the metal ion.[2b] While thorium is largely limited to the tetravalent oxidation state, the later actinides have a number of accessible oxidation states; plutonium can coexist in aqueous solution as Pu^{III}, Pu^{IV}, Pu^{V}, and Pu^{VI}. The tetravalent state in particular is the most Lewis acidic and thus +4 actinides (An = Th–Pu) are particularly prone to hydrolysis and condensation, with the formation of polynuclear species occurring under even very acidic conditions.[3c] Plutonium, for example, has been shown to form large polyoxo clusters ranging from $\{Pu_{16}\}$ to $\{Pu_{38}\}$ oligomers from acidic HCl solutions.[3a,d,e] Uranium and neptunium similarly form polyoxo clusters; these clusters are often stabilized by organic carboxylates.[3h,j,4]

Under aqueous conditions, hydrolysis and condensation reactions result in complex solution behavior of the actinides. The picture is further complicated by competing reactions—such as redox chemistry and ligand complexation—all of which are governed by solution conditions.[2b] For example, many An^{IV} metal cations ligated by carboxylate ligands have been isolated over the past ten years, ranging from mononuclear complexes to large polynuclear clusters capped and/or linked by organic ligands. However, the role of the complexing ligand in the assembly and stabilization of the structural units is somewhat unclear.[3b,h,j,5] Until relatively recently, it was generally accepted that organic carboxylates could be used to limit hydrolysis and condensation and thereby "trap" polynuclear species; however, examinations of aqueous Th perchlorate

[a] Dr. N. A. Vanagas, J. N. Wacker, D. R. C. Asuigui, Prof. S. L. Stoll, Dr. J. A. Bertke, Prof. K. E. Knope
Department of Chemistry
Georgetown University
37th and O Streets NW, Washington, D.C. 20057 (United States)
E-mail: kek44@georgetown.edu

[b] Dr. R. F. Higgins, Prof. E. J. Schelter
P. Roy and Diana T. Vagelos Laboratories
Department of Chemistry
University of Pennsylvania
231 S. 34th Street, Philadelphia, Pennsylvania 19104 (United States)

[c] E. Warzecha
Department of Chemistry and Biochemistry
Florida State University
Tallahassee, Florida 32306 (United States)

[d] J. N. Wacker, Dr. S. A. Kozimor
Los Alamos National Laboratory
Los Alamos, New Mexico 87545 (United States)

Supporting information (Structure refinement details; Thermal ellipsoid plots; Bond Valence Summation values; Powder X-ray diffraction patterns; UV/Vis-NIR spectra; Raman and IR spectra; TGA spectra; Magnetic data; TEM data) and the ORCID identification number(s) for the author(s) of this article can be found under: https://doi.org/10.1002/chem.201905759.

solutions showed that the assembly of hexanuclear units was dependent on the presence of organic carboxylates, with the ligand directing the assembly of the hexameric units from lower order (dinuclear) oligomers.[3b] Importantly, absent a complexing ligand, the hexanuclear units were not observed in solution or the solid state. Recent work in actinide-based metal–organic frameworks similarly provides evidence for the directing role of organic carboxylates, with the isolation of an unprecedented $An_6(\mu_3\text{-}O)_2$ structural unit, as opposed to the more common $An_6(OH)_4O_4$ core, stabilized within a hybrid extended network.[6] Indeed, several unique An species that were previously absent from descriptions of actinide structural chemistry have been observed through structural characterization of actinide-organic coordination polymers and metal–organic frameworks.[3g,7] Further, Mazzanti et al. recently stabilized $\{U_6\}$, $\{U_{16}\}$, $\{U_{24}\}$, and $\{U_{38}\}$-oxo clusters capped by benzoate ligands from organic solutions.[3j] Outside of providing further support for the utility of organic carboxylates in modulating the formation of actinide clusters, this work highlighted the importance of solution conditions on assembly and the time dependence of phase formation. Related to these efforts, our group has been investigating the directing effects of both charge balancing counterions and complexing ligands on the assembly of Th^{IV} and U^{IV} complexes.[8] Of particular interest with respect to the latter is the influence of the organic backbone and functionality on species formation, stabilization, and reactivity. More specifically, we are interested in understanding how changes in ligand sterics and coordination mode are manifested in the structural chemistry of metal complexes and clusters. In this work we examined the self-assembly of U^{IV}-2-furoate compounds in mixed solvent systems (H_2O/THF) with the aim of unraveling the effects of hydrolysis and condensation, ligand complexation, and solution conditions on species formation. The monoanionic ligand, 2-furoic acid (2-FA), was chosen for several reasons. 1) It contains functionalities, carboxylate and furoate, present in environmentally relevant species implicated in actinide mobility. 2) It is soluble in both water and tetrahydrofuran, which enabled us to tune the solution conditions without ligand precipitation, while also controlling hydrolysis and condensation through the systematic addition of water. 3) Its potential to form supramolecular interactions, such as hydrogen bonding and π–π stacking, may provide a facile route towards crystallization. 4) As compared to previous monoanionic carboxylates examined, most of which are simple amino acids or benzoate derivatives, it contains a furan ring that allows us to examine the effects of this structural modification on the resulting complexes.

These careful considerations led to the successful synthesis and characterization of five new U^{IV} compounds, reported herein. What is novel is that by limiting the M:L ratio, at low water concentrations, we were able to synthesize a compound consisting of 1D chains, $[UCl_2(2\text{-}FA)_2(H_2O)_2]_n$ (**1**). By simply changing the M:L ratio it was possible to control the nuclearity; a tetranuclear cluster $[U_4Cl_{10}O_2(THF)_6(2\text{-}FA)_2]\cdot 2\,THF$ (**2**) was observed at low water content. By increasing the water concentration the nuclearity could be increased to six as observed in $[U_6O_4(OH)_4(H_2O)_3(2\text{-}FA)_{12}]\cdot 7\,THF\cdot H_2O$ (**3**) and $[U_6O_4(OH)_4(H_2O)_2(2\text{-}FA)_{12}]\cdot 8.76\,H_2O$ (**4**). Over time, the high nuclearity cluster $[U_{38}Cl_{42}O_{54}(OH)_2(H_2O)_{20}]\cdot m\,H_2O\cdot n\,THF$ (**5**), was isolated. The crystal structures have been determined and reflect the tuning of the bonding and resulting structures by the synthetic conditions. We believe the oxidation state of all compounds is U^{IV}, and this conclusion is supported by UV/Vis absorption spectroscopy, and magnetic studies. Although the solventless thermolysis studies using TGA-DTA confirm that UO_2 is the stable product, we have been able to investigate the solution thermolysis to form ultra-small UO_2 nanoparticles. These studies lend insight not only to controlled hydrolysis and condensation, but also the transformation of uranium from soluble molecular species to nanomaterials.

Results and Discussion

It is well established that the crystallization and structure of metal organic materials depends largely on solution conditions including solvent system, pH, temperature, time, molar ratio of the reactants, presence of counter-ions, and pressure.[9] Variations of these parameters are known to influence the species that form. Reactions of U^{IV} with 2-furoic acid in a mixed H_2O/THF solvent system yielded five distinct U^{IV} phases. While the compounds isolated in this work exhibit some structural similarities with previously reported U^{IV} complexes and extended networks, notable differences exist in the surface decoration and overall connectivity of the structural units.

Structure descriptions and structural systematics

Compound **1**, $[UCl_2(2\text{-}FA)_2(H_2O)_2]_n$, crystallizes in the monoclinic space group *C*2/*c*. The structure is built from one crystallographically unique U^{IV} metal center, one chloride, one water molecule, and one distinct furoate ligand. As shown in Figure 1a, the U metal center is 8-coordinate bound to two Cl ions (Cl1 and $Cl1^{ii}$), two bound water molecules (O1 and $O1^{ii}$), and four oxygens (O11, O12, and their symmetry equivalents) from four bridging 2-FA. Adjacent metal centers are bridged through 2-FA units into 1D chains that propagate along the [0 0 1] (Figure 1b) with a U···U interatomic distance of 5.165(2) Å. Overall, the structure adopts a three dimensional supramolecular network through π–π stacking interactions of the furan rings with minimum $C_g\cdots C_g$ distances and slip angles of 3.470(1) Å and 16.4°, respectively.

The 1-dimensional chains observed in **1** are fairly unique within An^{IV} structural chemistry. Within Th^{IV} systems, a limited number of related linear chains have been isolated. For example, Hennig et al. reported a Th^{IV} glycine coordination polymer, wherein Th metal centers were linked by three bridging monodentate carboxylate groups from the glycine ligands.[10] Additionally, Loiseau et al. reported two polymorphic phases of $Th(Bz)_4$ (Bz = benzoate), wherein isolated Th metal centers were linked through the carboxylate groups of four bridging monodentate Bz ligands.[11] For U, the structure of $U(OAc)_4$ (OAc = acetate) consists of U^{IV} sites bridged by four acetate ligands, with one acetate exhibiting chelating and three acetates displaying bridging monodentate coordination modes.[12]

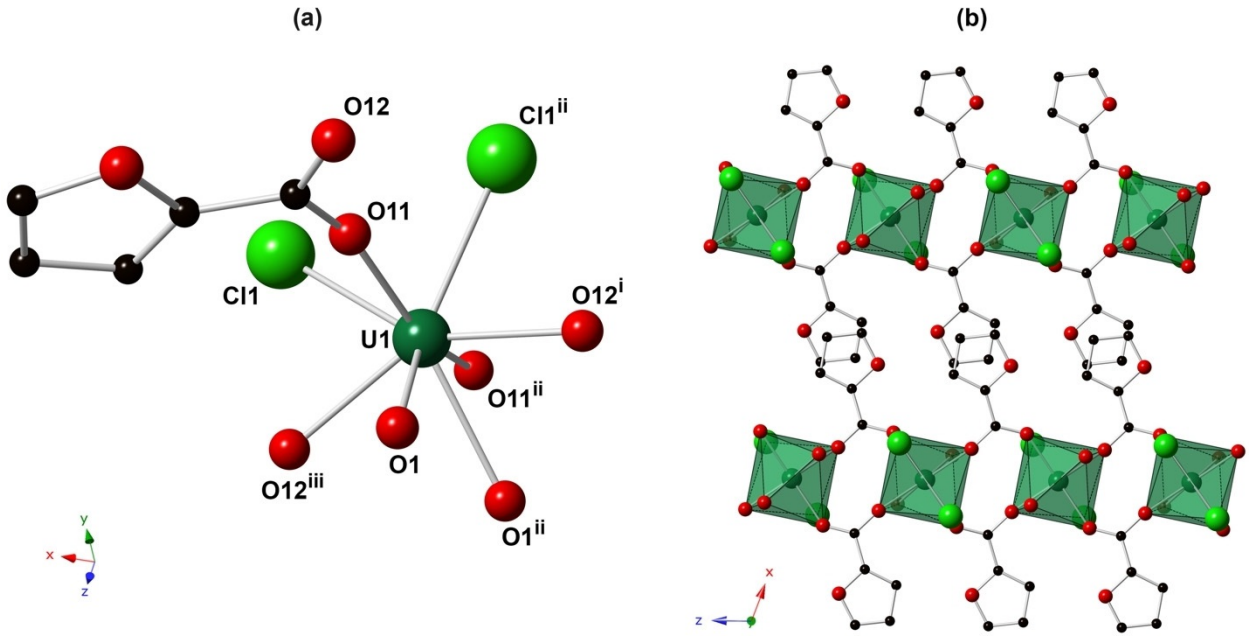

Figure 1. (a) Ball and stick representation of the local coordination sphere about the U^{IV} metal center in **1**. (b) Polyhedral representation of **1**, highlighting the ligand bridged 1D chains that extend along the [0 0 1]. Dark green, light green, red, and black spheres represent uranium(IV), chlorine, oxygen, and carbon atoms, respectively. Green polyhedra are 8-coordinate U^{IV}. Hydrogen atoms are not shown for clarity. Superscript denotes symmetry operators: i = $-x+1$, $-y+1$, $-z+1$; ii = $-x+1$, y, $-z+3/2$; iii = x, $-y+1$, $z+1/2$.

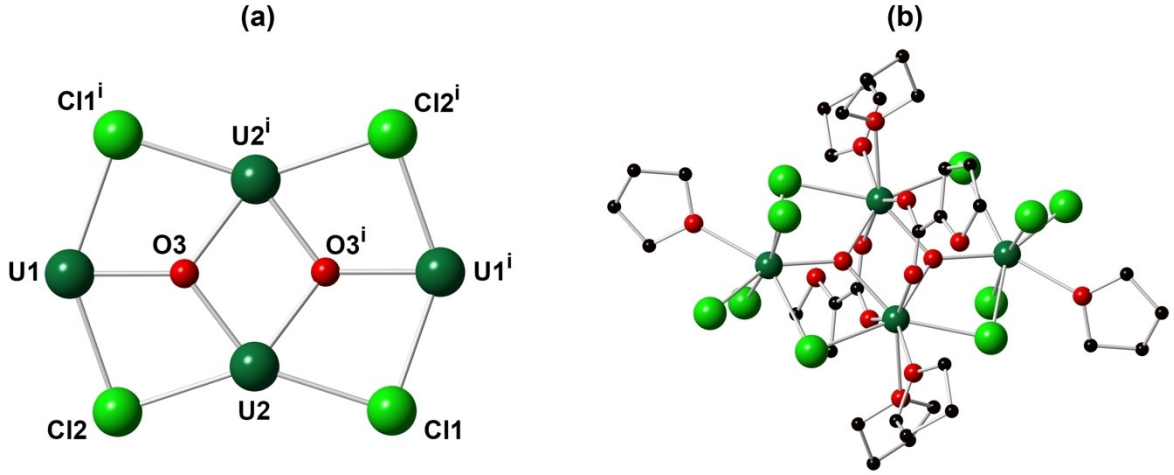

Figure 2. Ball and stick representation of (a) the tetranuclear $[U_4(\mu_3\text{-}O)_2Cl_4]^{8+}$ core and (b) the ligand decorated cluster in **2**. Dark green, light green, red, and black spheres represent U, Cl, O, and C atoms, respectively. Hydrogen atoms and disorder within the 2-FA ligands are omitted for clarity. Superscript denotes the symmetry operator: i = $1-x$, $2-y$, $1-z$.

By comparison the U^{IV}-carboxylate bridged chain reported here, with both chloride and carboxylate coordination as well as two bridging monodentate ligands linking metal centers, has not been reported.

Compound **2**, $[U_4Cl_{10}O_2(THF)_6(2\text{-}FA)_2]\cdot 2\,THF$, crystallizes in the monoclinic space group $P2_1/n$. The structure is built from two crystallographically unique U^{IV} metal centers, one distinct furoate ligand, four THF molecules, and five unique chloride ions. As shown in Figure 2, the U metal centers are bridged through μ_2-Cl and μ_3-O groups to form a tetranuclear cluster core of composition $[U_4(\mu_3\text{-}O)_2Cl_4]^{8+}$. Six chlorides and two 2-FA ligands cap the cluster to charge balance the octacationic core. Six THF molecules are additionally bound to the cluster (Figure 2b). U1 is seven coordinate, bound to five chloride ligands from three singly bound chlorides and two μ_2-Cl and two O atoms from one μ_3-O and one THF molecule. Alternatively, U2 is eight coordinate, bound to two μ_2-Cl and six O atoms from two THF molecules, two μ_3-O, and two O atoms from two bridging 2-FA ligands. Average U-μ_3-O, U–$O_{FA/THF}$, U-μ_2-Cl, and U–Cl distances are 2.22(2), 2.44(10), 2.80(2), and 2.62(2) Å, respectively. U1···U2 distances range from 3.967(2)–4.004(1) Å

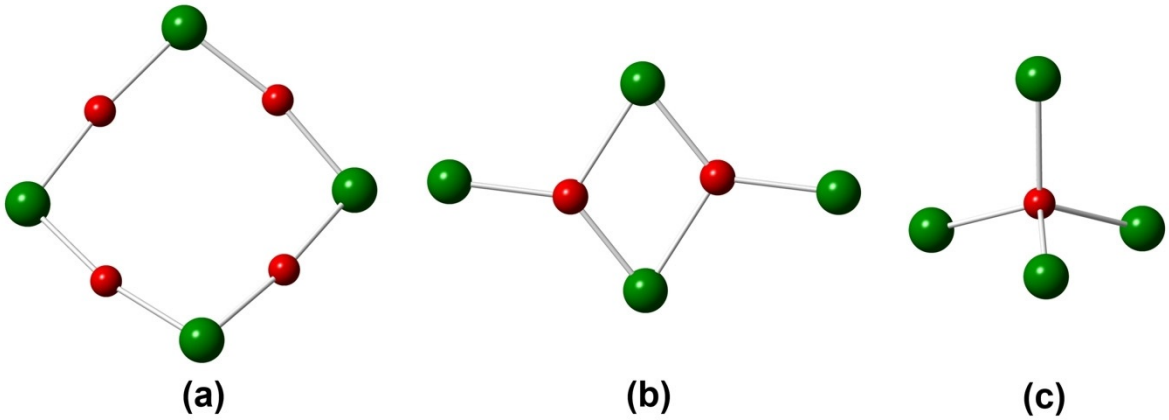

Figure 3. Illustration of the U^{IV}-oxo bridged tetranuclear cores observed in the solid state including (a) $[U_4O_4]^{8+}$,[14h] (b) $[U_4O_2]^{12+}$,[3g,14e,g] and (c) $[U_4O]^{14+}$.[15] The tetramer isolated in this work adopts the motif shown in (b). Only the U^{IV} metal centers (green spheres) and bridging O ligands (red spheres) are shown.

and U2···U2 distances are 3.5939(13) Å; the U1···$U1^{i}$ interatomic distance is 7.114(3) Å.

A limited number of homometallic tetramers, such as that observed in **2**, have been isolated for U^{IV}. A search of the Cambridge Structural Database (v 2.0.1) showed nineteen structures that consisted of tetranuclear cores, wherein the metal centers were bridged by Cl, N, and/or O.[13] The majority of these tetramers were stabilized by bulky ligands, with μ_2/μ_3-nitrogen atoms bridging the metal centers.[14] Only eight of the reported tetramers contained $\mu_2/\mu_3/\mu_4$-oxo groups and were found to adopt one of three unique structural units as shown in Figure 3.[3g,14e,g,h,15] The tetranuclear core observed in **2** (Figure 3b) is the most common of the tetramers with five other compounds adopting related structural units. By comparison, only two μ_2-oxo bridged cluster and one μ_4-oxo bridged structural unit such as those illustrated in Figure 3a and c, respectively, have been previously observed.

The structures of compounds **3** and **4** both consist of hexanuclear $[An_6O_4(OH)_4]^{12+}$ clusters that are built from six U^{IV} cations, four μ_3-OH, and four μ_3-O as shown in Figure 4. Such hexameric units are well known structural units in tetravalent metal ion structural chemistry. Related hexamers have been observed both in solution and the solid state across the early actinides for Th, U, Np, and Pu.[10,16] Though the hexanuclear $[U_6O_4(OH)_4]^{12+}$ units are nearly indistinguishable from those previously reported, differences in the binding modes of the carboxylate ligands with respect to the metal centers are observed. These variations in the surface decoration of the clusters are attributed to changes in the local coordination environment of each U^{IV} metal center. As such, ligand binding modes underpin the structural differences observed in **3** and **4**, as well as the other hexanuclear An^{IV}-carboxylates previously reported. The binding modes exhibited by 2-FA in **3** and **4** are shown in Figure 5.

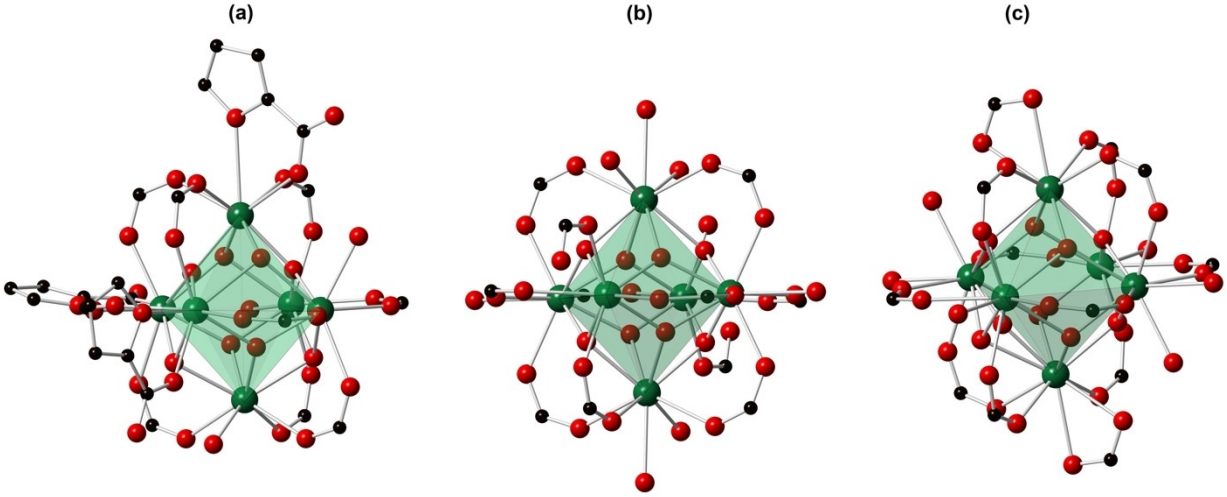

Figure 4. Illustration of the ligand decorated clusters in **3** (a) and **4** (b,c). Each cluster adopts a hexanuclear $[An_6O_4(OH)_4]^{12+}$ core; however, differences in the surface decoration of the clusters and variation in 2-FA bonding modes are attributed to changes in the local coordination environment of each U^{IV} metal center. Green, red, and black spheres represent uranium, oxygen, and carbon atoms, respectively. Green polyhedra highlight the hexanuclear cores. Only the furan ring of the 2-FA unit that binds via O atoms from both the carboxylate and furan ring is shown for clarity. Hydrogen atoms and the disorder of the 2-FA ligands are omitted.

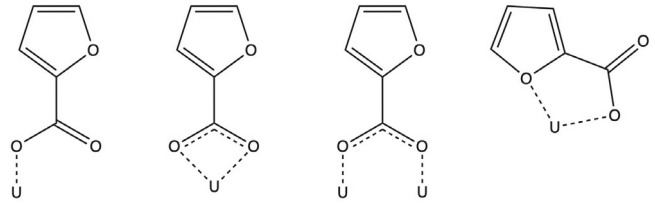

Figure 5. Binding modes of the 2-FA units observed in **3** (a,c,d) and **4** (b–d).

Compound **3**, $[U_6O_4(OH)_4(H_2O)_3(2\text{-FA})_{12}]\cdot 7\,THF\cdot H_2O$, crystallizes in the trigonal space group $P3_1c$. The structure is built from two crystallographically unique U^{IV} metal centers. U1 is 8-coordinate, bound to four μ_3-O/μ_3-OH, one bound water molecule, and three oxygen atoms from three monodentate 2-FA units. U2 is 9-coordinate bound to two μ_3-OH, two μ_3-O, and five oxygen atoms from four 2-FAs. Three of the ligands are bridging bidentate and link adjacent metal centers through the carboxylate oxygen atoms. Alternatively, one of the 2-FA ligands binds the metal center through one oxygen atom from the carboxylate and one oxygen atom from the furan ring with U–O bond distances of 2.394(8) and 2.854(1) Å, respectively. U–O and U···U distances range from 2.170(9)–2.854(10) and 3.764(1)–3.879(1) Å, respectively.

Compound **4**, $[U_6O_4(OH)_4(H_2O)_2(2\text{-FA})_{12}]\cdot 8.76\,H_2O$, crystallizes in the triclinic space group $P\bar{1}$. The structure is built from six crystallographically unique U^{IV} metal centers. Each of the U^{IV} sites exhibits a unique coordination environment and overall, there are two unique $[U_6O_4(OH)_4(H_2O)_2(2\text{-FA})_{12}]$ clusters within the structure. The first cluster is composed of U1–U3 and their symmetry equivalents. U1 and U3 are nine-coordinate. U1 is bound to three water molecules, four μ_3-O/μ_3-OH, and one bridging 2-FA. U3 is bound to one water molecule, four μ_3-O/μ_3-OH, and four bridging 2-FA. Alternatively, U2 is eight-coordinate bound to four μ_3-O/μ_3-OH, three bridging 2-FA, and one monodentate 2-FA. U–O bond distances range from 2.129(22) to 2.743(26) Å, with the shortest corresponding to a U-μ_3-oxo bond and the longest corresponding to a U-H_2O bond. The bridging 2-FA link adjacent U sites with U···U distances ranging from 3.787(5)–3.886(3) Å. The second cluster is built from U4–U6 and their symmetry equivalents. In contrast to the cluster described above, all of the U sites are nine-coordinate. Each of the U^{IV} metal centers are bound to four μ_3-O/μ_3-OH groups. One chelating 2-FA and three bridging 2-FA units additionally ligate U4. U5 is bound to one water molecule and four bridging 2-FA units. U6 is bound to two water molecules and three bridging 2-FA units. U–O and U···U distances range from 2.189(24)–2.732(26) and 3.805(4)–3.904(3) Å, respectively.

Compound **5**, $[U_{38}Cl_{42}(OH)_2O_{54}(H_2O)_{20}]\cdot m\,H_2O\cdot n\,THF$, crystallizes in the tetragonal space group, $I4/m$. Overall, the structure is built from a $[U_{38}O_{54}]^{44+}$ cluster core related to those previously reported by the groups of Mazzanti and Loiseau for U^{IV}, Loiseau for Np^{IV}, and Soderholm, Burns, and Hixon for Pu^{IV}.[3d,e,j,4,17] Previously reported U_{38} cluster cores have been isolated with various carboxylate, chloride, and/or acetamide ligands. In contrast, the cluster reported herein is exclusively capped by chloride anions and water molecules, with forty two chlorides and twenty water molecules decorating the surface (Figure 6). Related chloride and water ligation has been observed for the three $[Pu_{38}O_{56}]^{40+}$ clusters previously reported, which all have different amounts of water and chloride bound to the surface. As in previous An_{38} clusters, the 38 U atoms that constitute the core in **5** adopt the fluorite structure, with distortions away from the ideal $Fm3m$ symmetry. As similarly described by Loiseau for previous U_{38} clusters,[3h,18] seven crystallographically unique metal centers constitute the U_{38} core in **5**; each metal center is eight coordinate and adopts a distorted square antiprism coordination geometry. As shown in Figure 6, fourteen U^{IV} sites occupy the center of the cluster, with the eight metal sites at the corners of the cluster ligated by water molecules. This $\{U_{14}\}$ unit is capped on each of the six faces by a $\{U_4\}$ structural unit to give the $\{U_{38}\}$ cluster core. There are two distinct $\{U_4\}$ structural units, denoted $\{U_4\}$-1 and $\{U_4\}$-2 in Figure 6. {U4}-1 consists of four crystallographically equivalent U^{IV} sites that are each bound to one terminal chloride, two μ_2-bridging chlorides, and one μ_4-chloride in addition to the four O atoms that are shared with the $\{U_{14}\}$ core. {U4}-2 is built from four U^{IV} sites (three are crystallographically unique) where each U is eight-coordinate. Each U atom is bound to four O atoms, connecting it to the $\{U_{14}\}$ core; however, three of the U^{IV} sites are additionally bound to one terminal water, two μ_2-bridging chlorides, and one μ_4-chloride, whereas the remaining U center is ligated by one terminal chloride, two μ_2-bridging chlorides, and one μ_4-chloride. Average U–O bond lengths for U-μ_3-O, μ_4-O, and H_2O are 2.25(4), 2.36(4), and 2.53(6) Å, respectively. Average U–Cl bond lengths for U-μ_2-Cl, μ_4-Cl, and terminal Cl are 2.83(1), 3.05(1), and 2.71(1) Å, respectively. U···U interatomic distances within the cluster range from 3.586(2)–3.947(1) Å.

With respect to the reported formula for **5**, bond valence summation (BVS) values were calculated for the seven crystallographically unique uranium centers.[19] The values ranged from 3.920 to 4.186 consistent with U^{IV} (Table S1 in Supporting Information). BVS values were also calculated for the 56 μ_3-/μ_4-oxygen atoms that constitute the core as well as the twenty water molecules that bind the surface of the cluster (Table S2). The values for the μ_3-/μ_4-O ranged from 1.98 to 2.11 and are consistent with assignment of these sites as oxo groups. The values for the H_2O sites ranged from 0.28–0.39 and are consistent with assignment of these sites as water molecules. However, this would lead to a formula of $[U_{38}Cl_{42}O_{56}(H_2O)_{20}]^{2-}$ with a net anionic charge. We considered three possibilities to charge balance the cluster: 1) presence of U^V in the cluster to give $[U^{IV}{}_{36}U^V{}_2Cl_{42}O_{56}(H_2O)_{20}]$, 2) partial occupancy of H_2O on the terminal chloride sites to give $[U_{38}Cl_{40}O_{56}(H_2O)_{22}]$, and 3) protonation of two of the twenty-four μ_3-oxo sites to give $[U_{38}Cl_{42}(OH)_2O_{54}(H_2O)_{20}]$. The magnetic data and absorption spectrum for **5** showed little evidence for U^V. To examine the possibility of partial occupancy or substitution of H_2O for Cl, the surface Cl sites were parted into two sites (O and Cl), assigned a free variable, and the occupancy was allowed to freely refine. In all cases, the occupancy of Cl refined to 1; dis-

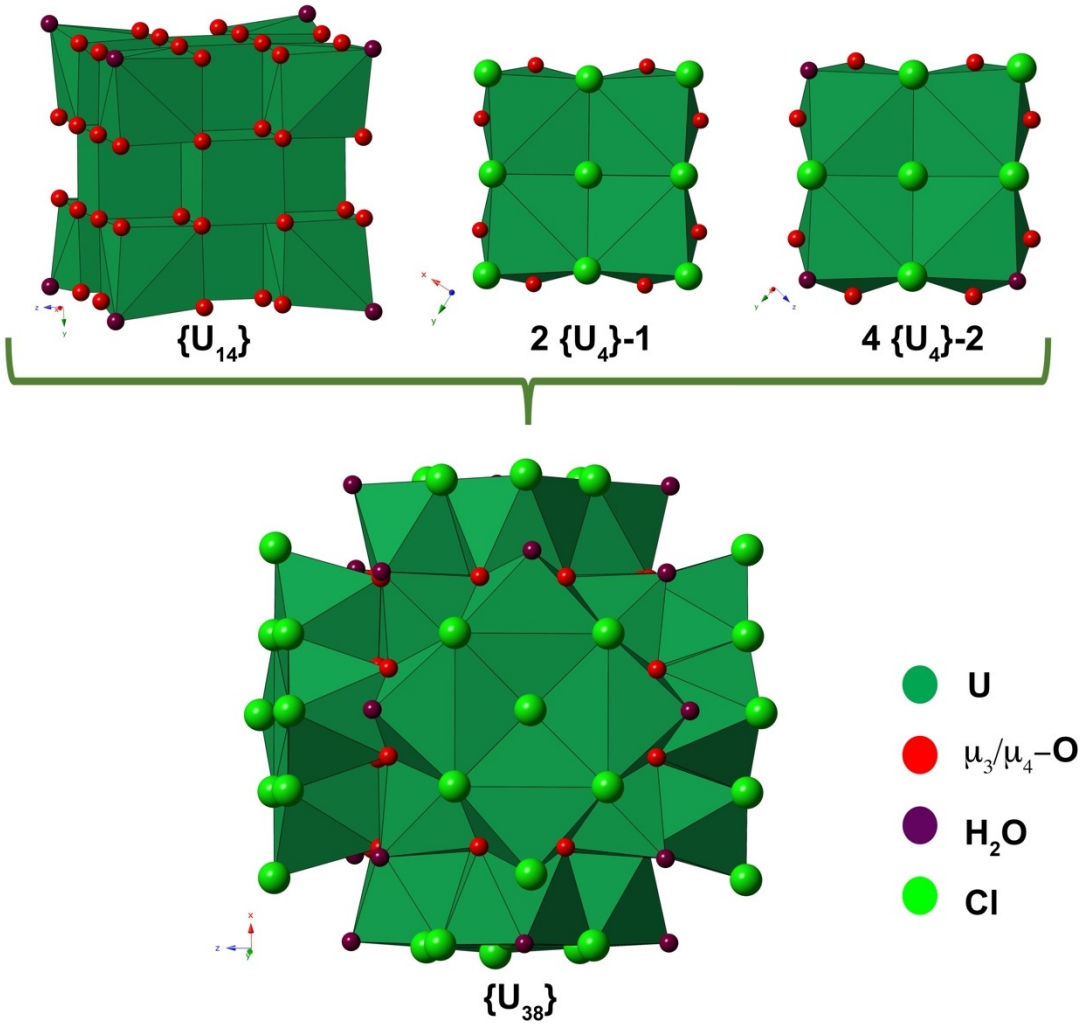

Figure 6. Polyhedral representation of **5** showing the chloride and water decorated U_{38}-oxo cluster. The cluster core is built from a $\{U_{14}\}$ core that is capped by six $\{U_4\}$ units. There are two distinct $\{U_4\}$ moieties; the face of $\{U_4\}$-1 consists of nine chloride ligands while the face of $\{U_4\}$-2 is ligated by six chlorides and three water molecules. Green polyhedra are 8-coordinate U^{IV} metal centers. Red, purple, and light green spheres represent oxygen, water, and chloride, respectively.

ordering of the terminal Cl sites with H_2O resulted in an unsatisfactory refinement. With respect to the third possibility, the disordering of μ_3-OH/O has been observed for hexanuclear clusters.[3f,8a,18] In many cases, the disordered sites have U–O bond distances intermediate (2.34–2.37 Å) those of U-μ_3-O (2.19–2.28 Å) and U-μ_3-OH (2.42–2.48 Å).[3f,8a,18] For example, in **4** the U-μ_3-O/OH bond distances were found to be 2.35(2) Å, consistent with partial (50%) occupancy of μ_3-O and μ_3-OH. For **5** there are no discernable differences in the bond distances that would allow us to assign one of the sites as a hydroxide group. Moreover, as the OH sites may be disordered over several sites, have a low occupancy, and low electron count, it was not possible to determine the OH sites. Based on the above considerations we thus arbitrarily formulated the cluster as $[U_{38}Cl_{42}(OH)_2O_{54}(H_2O)_{20}]$.

As **5** was isolated from aging of the solution that yielded **2**, it is worth considering the relationship between the tetranuclear cluster in **2** and the U_{38} cluster in **5**. While it is possible that the tetramers in **2** assemble together with larger oligomers to form the U_{38} cluster, the tetranuclear core in **2** is distinct from the $\{U_4\}$ units that cap the $\{U_{14}\}$ core to yield $\{U_{38}\}$ as depicted in Figure 6. Moreover, to the best of our knowledge, a $\{U_{14}\}$ cluster akin to that observed in the U_{38} cluster has not been observed for the tetravalent actinides thus far. Though a polyoxo $\{U_{14}\}$ cluster was recently reported, it differs significantly from the core unit in the U_{38} cluster.[20] For related Pu_{38} clusters, Hixon et al. recently proposed that $\{Pu_{16}\}$ and $\{Pu_{22}\}$ are building blocks for Pu_{38},[3a] and gas phase studies by Gibson and Haire show evidence for Pu_6 and Pu_{16} species.[21] Consistent with this, Loiseau et al. have recently isolated $\{U_{12}\}$ and $\{U_{14}\}$ clusters and proposed that polyoxo clusters may assemble through the condensation of $U_6O_4(OH)_4$ species with dinuclear units such that "$6+2n$" nuclearity units, where $n=1$–6, may be accessible.[20] Mazzanti and Hixon isolated $\{An_{16}\}$ units for U and Pu, respectively, but these clusters differ significantly from those reported by Loiseau et al. due in part to differences in the U^{IV} coordination environment.[3a,j] Still, it re-

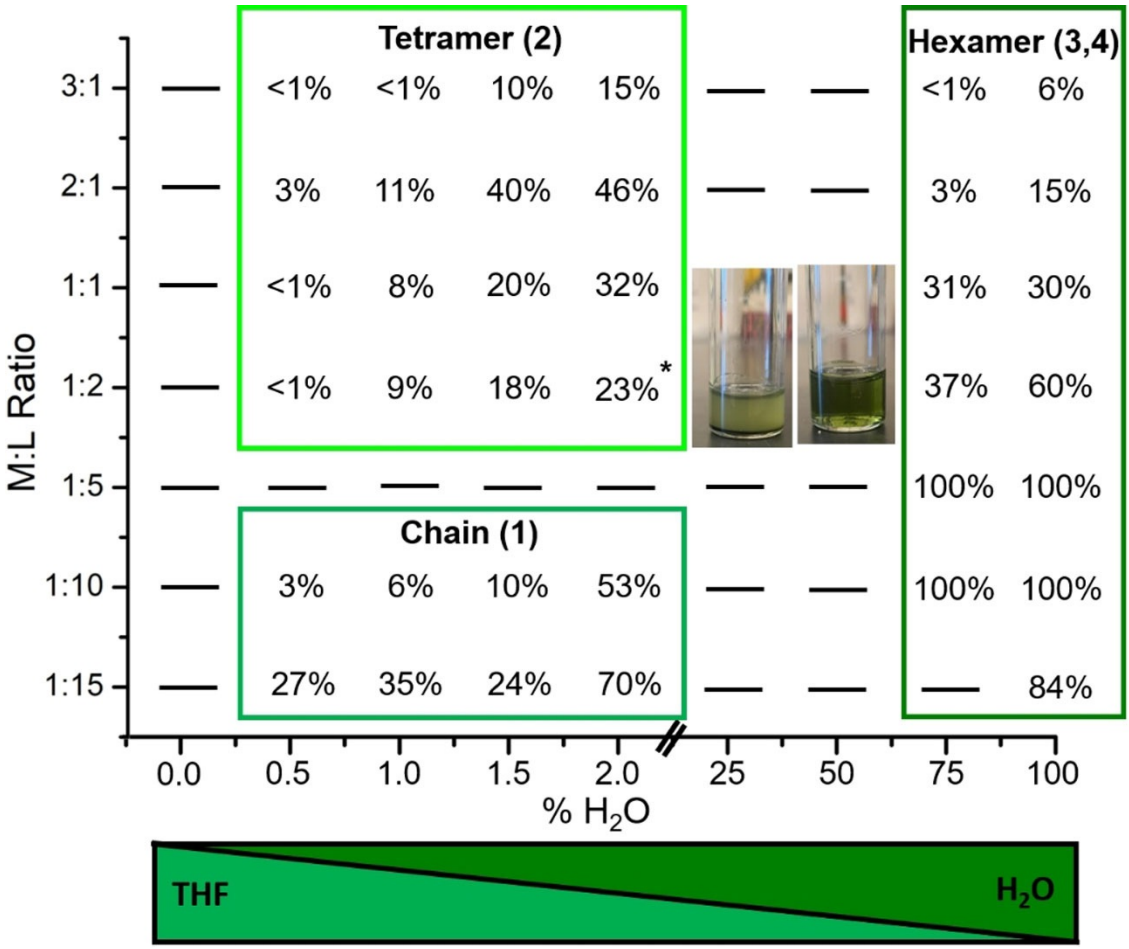

Figure 7. Illustration of the synthetic space over which **1**–**4** were isolated and corresponding percent yields. Note that compound **5**, which consists of large polynuclear U_{38} clusters, was isolated upon aging of the solution marked with an *.

mains unclear how the $\{U_4\}$ units isolated in this work relate to these larger oligomers and the $\{U_{38}\}$ cluster, in particular.

Synthetic considerations

Reaction conditions such as pH, temperature, time, and concentration are known to influence product formation.[3j,9,18] U^{IV}-2-FA phase formation was thus explored as a function of synthetic conditions (e.g., THF/H_2O and U:2-FA ratios and reaction time and temperature). Figure 7 summarizes the synthetic space that was explored and the compounds that were isolated at various metal to ligand ratios and in different solvent systems. It is worth noting that compounds **1**–**4** were observed over a wide temperature range (25–80 °C); however, the optimal temperature in terms of yield and crystal quality was found to be 50 °C. Controlling the amount of water in the reaction solution allowed for the examination of the hydrolysis and condensation behavior of U^{IV} in the presence of 2-FA. At a 1:1 stoichiometric ratio of U^{IV} and 2-FA, different products were observed with increasing water concentration. For example, as shown in Figure 7, at low water content (0.5–2% H_2O) tetrameric species (**2**) were observed. Between 3 and 25% H_2O, no precipitate formed; however, a clear separation between the dark green water layer (bottom) and the cloudy THF layer appeared; Raman spectra collected for the water layer showed no evidence of THF and similarly the THF layer showed no peaks attributed to water. Such a separation was not observed for solutions with increasing water concentration (e.g., 60% THF/40% H_2O) but still no precipitate was evident. At 75% H_2O; however, a new phase (**3**) consisting of hexanuclear clusters was isolated. Upon increasing the water concentration further, another hexanuclear species (**4**) was observed, with differences between the structural units in **3** and **4** attributed to the solvent system. The increase in nuclearity that is observed from the tetrameric species in **2** at lower water content compared to hexameric units in **3** and **4** at higher water content is consistent with expected trends in hydrolysis and condensation. Indeed, a number of related hexanuclear An^{IV}-carboxylate clusters have been isolated from aqueous solution under relatively similar reaction conditions.[3b,5b,8a]

The formation of oligomers has been shown to result from a delicate interplay of hydrolysis and condensation as well as ligand complexation. Recent literature has shown that organic ligands may be used to thwart hydrolysis and condensation, stabilize novel structural units, or otherwise direct the assembly of larger order oligomers from smaller order polynuclear

species.[3a,j,17] As such, the effects of metal/ligand ratios on phase formation were examined. Upon increasing the metal/ligand ratio at low water concentrations from 1:1 to 2:1, the yield of **2** was found to increase. This may be expected as this corresponds to the stoichiometric ratio found in the product. However, upon increasing the ligand concentration (1:5 to 1:15) a new phase (**1**) consisting of ligand-bridged mononuclear species was observed. This result suggests that in the presence of a large excess of ligand, complexation may compete with hydrolysis and condensation and thereby thwart the formation of polynuclear hydroxo/oxo bridged species. Mazzanti et al. have shown that an increase of capping ligand in solutions that otherwise yielded ligand decorated $[U_6(OH)_4O_4]^{12+}$ cores resulted in the formation of a planar ligand capped $[U_6O_4]$ structural units.[3j] For **3** and **4**, the metal/ligand ratio was found to have little effect on the nuclearity of the resulting complexes or phase formation. The percent yields for both **3** and **4**; however, were found to increase with increasing ligand concentration, with excess ligand (1:5–1:10) giving near quantitative yields (based on U) for **3** and **4**.

Recent work, particularly on the formation of metal–organic frameworks, has examined the role that reaction conditions have on phase formation. Efforts in metal carboxylates, in particular, have shown the time dependent formation of various phases, with changes in local coordination environment of the metal ion, coordination number/mode of the carboxylate group, and ligand substitutions giving rise to structural changes.[9a] Similarly, for tetravalent uranium, Mazzanti et al. recently illustrated that the isolation of different size clusters from the same solution was time dependent, with $\{U_6\}$ forming after several hours, $\{U_{16}\}$ after several days, and $\{U_{24}\}$ after several weeks.[3j] In the present work, yields were found to increase with increasing reaction time for **1**, **3**, and **4** for solutions with metal/ligand ratios that correspond to the stoichiometry observed in the crystalline product. For example, whereas the yield for **3** was roughly 37% after twenty-four hours, after four days the yield was upwards of 70%. This may be attributed the formation of the clusters over a longer reaction time. By comparison, aging of the solution that yielded **2**, resulted in no appreciable increase in yield. Rather, prolonged reaction times (3–5 months) yielded the U_{38} cluster observed in **5**. Importantly, it was determined that 2-FA is necessary for the formation of **5** as no precipitate was observed when UCl_4 was dissolved in 99.5% THF/0.5% H_2O and heated at 50 °C over five months. Here exchange of the 2-FA ligand with Cl likely modulates the formation of the larger polyoxo clusters as has been observed previously.[3d,j,18]

Reaction temperature is similarly well known to influence product formation.[3f,8a] Compounds **2**–**4** were observed over a wide temperature range, 25–80 °C, though as mentioned previously the optimal temperature for crystallization and product yield was found to be 50 °C. By comparison, compound **1** was only observed above ambient temperatures. Heating the solutions from which **1**–**4** crystallized above 100 °C (**1**–**3**) or 120 °C (**4**) resulted in a color change consistent with the formation of UO_2 nanoparticles as has been previously reported.[3f,8a] Indeed, the powder X-ray diffraction was consistent with the formation of UO_2 (Figures S11–S14 in Supporting Information). Although this confirms that the only crystalline product from the solution thermolysis was UO_2, there is significant line broadening of the diffraction peaks. Based on the transmission electron microscopy (TEM), it is clear that the nanoparticles have quite distinct lattice fringes that correspond to the {111} lattice planes for $d \approx 3.1$ Å of UO_2 indicative of high crystallinity (Figure 8 and Figures S61–S68); the small size of the particles is consistent with the extremely broadened powder diffraction patterns. The particle sizes based on TEM (histograms of 60–67 particles), were 1.8 ± 0.3, 2.3 ± 0.3, and 2.5 ± 0.2 nm for nanoparticles formed from **1** (1D chains), **2** (tetrameric species) and **4** (hexamer), respectively. Interestingly, while the solution conditions for the molecular compounds could be carefully controlled to determine nuclearity of the resulting compound, under nanoparticle synthetic conditions there was very little variability in the particle size. In addition, time, temperature and concentration also appear to have little effect. This suggests that Oswald ripening is not occurring and may indicate a special stability for the species close to 2 nm in diameter.

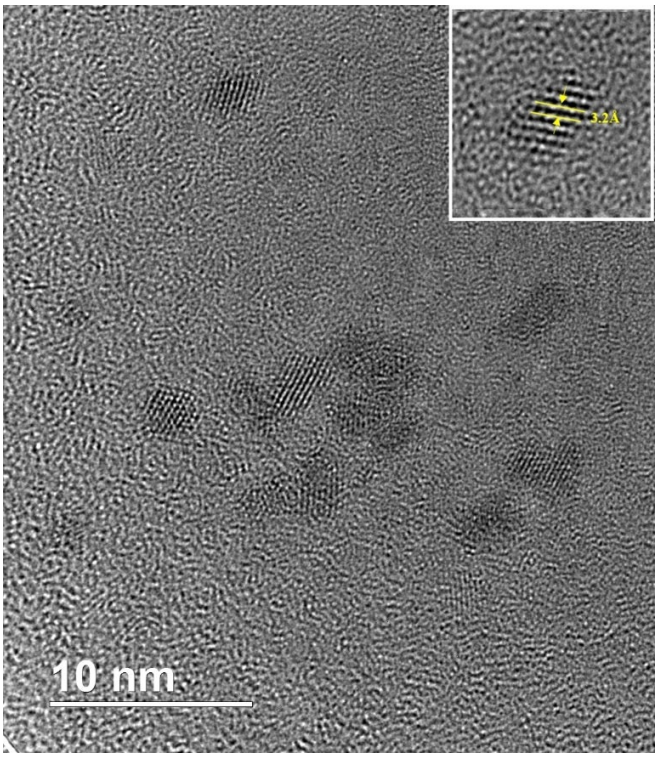

Figure 8. TEM image of the UO_2 particles that formed upon heating the reaction solution that yielded **2**. Inset shows *d*-spacing of 3.2 Å for a single particle.

Magnetism

U^{IV} and U^{V} are paramagnetic ions and magnetic susceptibility measurements are commonly used for characterizing the oxidation state of uranium complexes and clusters.[22] Solid-state magnetic susceptibility data were thus collected for **1**–**5** and used to assess the oxidation state of the synthesized com-

pounds. These data are shown in Figure 9 and are consistent with U^{IV} for all of the phases reported.

For compound **1**, $[UCl_2(2\text{-FA})_2(H_2O)_2]_n$, which consists of ligand bridged U^{IV} chains, at 300 K, the $\chi_M T$ value was 0.70 emu K mol^{-1} and decreased to almost zero at 2 K, where the magnetic susceptibility value was 0.02 emu K mol^{-1}. These data indicate little excited-state populations at low temperature and are consistent with ground-state singlet U^{IV} character. A saturation experiment performed at 2 K indicated a magnetization value of 0.09 μ_B at an applied field of 70 kOe, which confirms the assigned oxidation state of U^{IV} for this coordination polymer.

The $\chi_M T$ value at 295 K for **2** which consists of tetranuclear clusters was 3.77 emu K mol^{-1} (0.94 emu K mol^{-1} per U-ion), which decreases monotonically upon lowering the temperature until ≈75 K where the decrease becomes more pronounced. At 2 K, the $\chi_M T$ value attained was 0.31 emu K mol^{-1} (0.08 emu K mol^{-1} per U-ion). These data are typical of U^{IV} ions in low symmetry environments, which, upon decreasing the temperature attain a ground-state singlet.[22] These properties are similar to our previously reported hexanuclear U^{IV} cluster capped by 4-hydroxybenzoate ligands.[8a] To further confirm the singlet ground state for this cluster, a saturation of magnetization experiment was performed at 2 K, which yielded a magnetization value of 1.04 μ_B (0.26 μ_B per U ion) at an applied field of 70 kOe (Figure S37 in Supporting Information). These data were consistent with the presence of four ground-state singlet U^{IV} ions.[22,23]

Compounds **3** and **4**, both of which consists of hydrated hexanuclear clusters, display similar, but reduced, variable temperature magnetic susceptibility behavior as compared to $[U_4Cl_{10}O_2(THF)_6(2\text{-FA})_2]$ (**2**). For clarity, only the properties for **3** are discussed as the analyses for both phases consisting of hexanuclear units are nearly indistinguishable. For **3**, a room temperature magnetic susceptibility value of 3.34 emu K mol^{-1} (0.56 emu K mol^{-1} per U-ion) was observed, which decreased as the temperature was lowered until 2 K where a $\chi_M T$ value of 0.30 emu K mol^{-1} (0.05 emu K mol^{-1} per U-ion) was observed (Figure 9). A saturation magnetization experiment at 2 K showed a value of 0.82 μ_B (0.14 μ_B per U ion) with an applied field of 70 kOe (Figure S38). While the temperature dependent susceptibility values were low, they are reasonable considering other reported U^{IV} species and are reproducible over multiple batches (Figures S51 and S55).[22] Further, the small magnetization values obtained from saturation magnetization experiments support the presence of only U^{IV} ions for both clusters. Finally, small room temperature magnetic susceptibilities have been observed previously with oxygen atom bound U^{IV}[3h] and U^{V}[24] clusters.

Finally, the large U_{38} cluster displayed data quite typical for U^{IV} ions. The per-U ion room temperature $\chi_M T$ value was 1.41 emu K mol^{-1} that decreased across all temperatures until 2 K, where the value was 0.02 emu K mol^{-1}, consistent with a ground state singlet. The larger increase in the susceptibility value with increasing temperature for **5** compared to the clusters **1**–**4** could be due to structural differences since **5** contains no carboxylates bound to the U^{IV} ions. At 300 K, **5** showed a $\chi_M T$ value of 1.41 emu K mol^{-1}, which is similar to room temperature $\chi_M T$ values for other halide/oxo U^{IV} samples such as UCl_4 and UOI_2 (1.35 and 1.39 emu K mol^{-1}, respectively).[22] This assignment of all U^{IV} ions for this cluster is supported by a saturation experiment performed at 2 K where at 70 kOe a value of 3.75 μ_B (0.10 μ_B per U ion) was observed, which lacked saturation of magnetization.

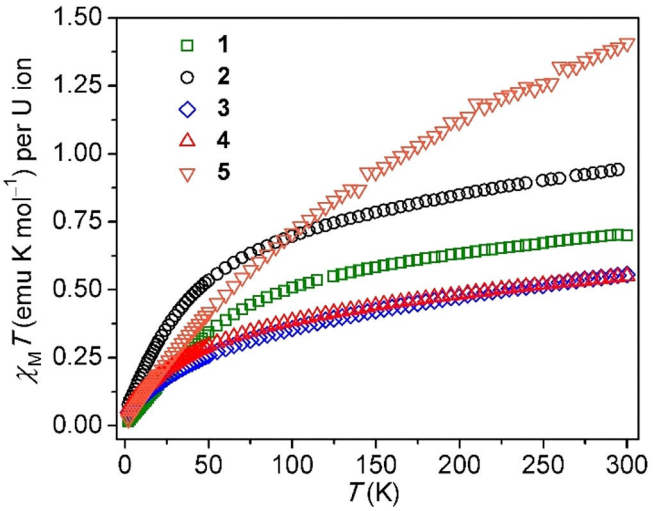

Figure 9. Temperature dependence of per-U ion magnetic susceptibility for (**1**) $[UCl_2(2\text{-FA})_2(H_2O)_2]_n$ (green squares); (**2**) $[U_4Cl_{10}O_2(THF)_6(2\text{-FA})_2]$ (black circles); (**3**) $[U_6O_4(OH)_4(H_2O)_3(2\text{-FA})_{12}]$ (blue diamonds); (**4**) $[U_6O_4(OH)_4(H_2O)_2(2\text{-FA})_{12}]$ (red triangles), and (**5**) $[U_{38}Cl_{42}O_{54}(OH)_2(H_2O)_{20}]$ (orange inverted triangles).

UV/Vis-NIR Spectroscopy

Characteristic f–f transitions from the $^3H_4$ ground state dominate the electronic absorption spectrum of tetravalent uranium, thereby providing a powerful handle for oxidation state determination. More recently, UV/Vis-NIR spectroscopy has also been used with some success to identify the nuclearity of structural units in solution by correlating solution features with the solid-state absorbance bands, but current reports are restricted to monomeric and hexameric structural units. Given the limited number of published absorption spectra of U^{IV} complexes and larger polynuclear species, in particular, the optical spectra of **1**–**5** were collected in an effort to confirm oxidation state and understand spectral changes that may occur as a function of ligand decoration and/or metal-oxo cluster nuclearity. The reported compounds display a systematic increase in cluster size, from small tetrameric and hexameric oligomers to large clusters, while exhibiting similar ligand decoration and as such provide a catalog of U^{IV} compounds that can be used to assess the influence of factors such as nuclearity on the U^{IV} absorbance spectrum. Coordination environment, coordination number, and the solvent identity have similarly been shown to influence the observed transitions, thereby leading to changes in the peak position and relative intensity of the absorption bands;[3g,8d,25] these factors were also taken into consideration and are discussed below.

The solid-state UV/Vis absorption spectra of compounds **1**–**5** are all consistent with tetravalent uranium, but exhibit slight shifts in the energy, relative intensities, and splitting of the observed bands (Figures 10 and 11). The absorption spectrum of a reference compound, $[U(H_2O)_4Cl_4]\cdot 2\,HPyCl$ (HPy = pyridinium), that consists of mononuclear U^{IV} units is shown for comparison as it is representative of limited nuclearity complexes.[8d] By comparison, the optical spectrum collected for compound **1**, which consists of ligand-bridged chains of mononuclear units, exhibits increased splitting relative to both the reference compound as well as the other phases presented herein, particularly in the region from 575–700 nm. Bands in this region are attributed to the $^3H_4\rightarrow{}^3P_0$, $^3H_4\rightarrow{}^1G_4$, and $^3H_4\rightarrow{}^1D_2$ transitions;[26] however, unique assignment of these bands is nontrivial due to the overlap and splitting of the peaks. To the best of our knowledge, the optical spectra of ligand bridged one-dimensional U^{IV} chains have not been reported previously. Shifts in the absorption bands in the optical spectra of closely related 3D frameworks built from mononuclear metal centers bridged by isophthalate or pyromellitate ligands have been observed and are attributed to changes in the coordination environment around the uranium metal centers,[25] yet the degree of splitting observed for **1** is fairly unique for higher coordinate U^{IV} complexes and extended networks.

Compound **2** contains tetrameric structural units and the optical spectrum exhibits more intense and broader peaks centered at 634, 660, and 678 nm attributed to the $^3H_4\rightarrow{}^3P_0$, $^3H_4\rightarrow{}^1G_4$, and $^3H_4\rightarrow{}^1D_2$ electronic transitions, respectively. The bands at 468, 503, and 554 nm may be assigned to terms $^3H_4\rightarrow{}^3P_2$, $^3H_4\rightarrow{}^1I_6$, and $^3H_4\rightarrow{}^3P_1$. This optical spectrum is fairly consistent with that of a previously reported U^{IV}-tetranuclear species decorated by formate and benzenedicarboxylate ligands,[3g] however, shifts in the peaks in the two spectra are likely attributed to the differences in U coordination environment and solvent effects. Compounds **3** and **4** both contain hexanuclear motifs. Such hexanuclear $U_6(OH)_4O_4$ clusters have been previously reported and the optical spectra of these phases are typically characterized by three electronic transitions, $^3H_4\rightarrow{}^3P_0$, $^3H_4\rightarrow{}^1G_4$, and $^3H_4\rightarrow{}^1D_2$, between 610–690 nm, with both the splitting and ratio of the intensities of the bands centered at ≈650 and ≈660 nm providing signatures for the hexanuclear unit; hexameric clusters are likely present when the ratio of the peaks is less than 1.[3f,5b,8a] The optical spectrum of **4** is consistent with these results, and hence characteristic of hexameric units, with the peak at 664 nm more intense than the band centered at 650 nm. The optical spectrum of **3** exhibits notable differences from that of **4** as well as previous reports of hexamers. In particular, the peak centered at 651 nm ($^3H_4\rightarrow{}^1G_4$) is relatively more intense than the band at 672 nm ($^3H_4\rightarrow{}^1D_2$). In looking to the crystal structure, both differences in metal-ligand binding as well as solvent incorporation are observed. To examine the effects of the latter, **3** was heated at 100 °C for 60 minutes to remove lattice solvent (Figure S29). The optical spectrum was subsequently collected (Figure S18) and the absorption bands more closely resembled those in the spectrum of **4**, with the peak at 671 nm slightly more intense than the band centered at 648 nm. These results suggest that the differ-

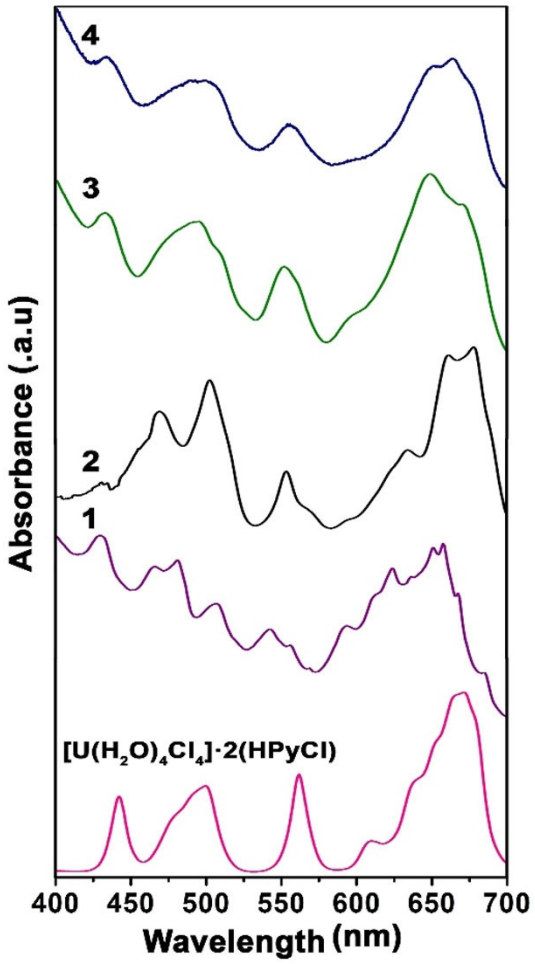

Figure 10. Solid-state UV/Vis spectra for compounds **1**–**4**. The mononuclear compound, $[U(H_2O)_4Cl_4]\cdot 2\,HPyCl$ (HPy = pyridinium), has been provided for reference to highlight the differences in the spectra as a function of nuclearity, ranging from mononuclear complexes to polynuclear clusters.

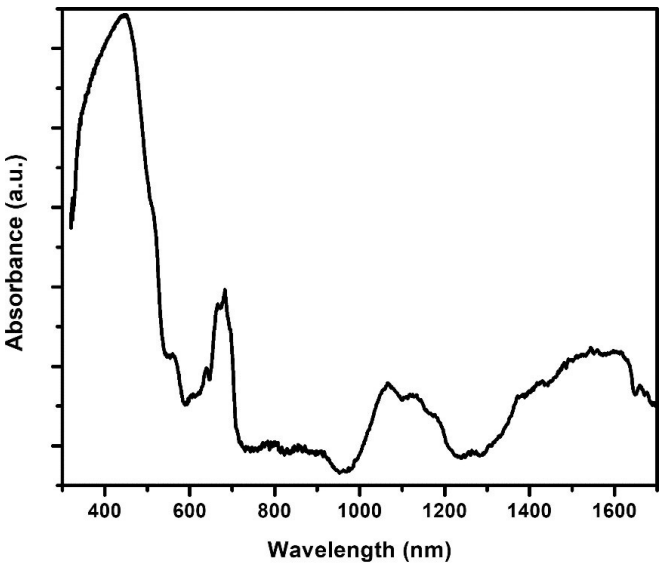

Figure 11. Solid-state UV/Vis-NIR absorption spectrum of **5**.

ences in the spectra of **3** and **4** are attributed largely to solvent effects.

To the best of our knowledge, the solid-state optical spectra of phases containing U_{38} clusters have not been previously reported. As shown in Figure 11, the optical spectrum of **5** is characterized by an intense broad band centered at 450 nm likely attributed to a charge transfer transition. Other, relatively weaker peaks are resolved at 525, 568 ($^3H_4 \rightarrow {}^3P_1$), 639 ($^3H_4 \rightarrow {}^3P_0$), 663 ($^3H_4 \rightarrow {}^1G_4$), and 682 ($^3H_4 \rightarrow {}^1D_{2)}$ nm and are characteristic of U^{IV}.

Given the differences in the solid-state optical absorption spectra of **1**–**5**, the optical spectra were collected on the solutions from which the compounds crystallized in an effort to assess the correlation between solution and solid-state structural units. The solution optical spectra were thus collected right before crystallization and compared to the solid-state spectra (Figures S15–17, S19, S20). While the solid-state spectra of **3** and **4** closely paralleled the solution spectra, indicating that the hexameric units assemble in solution before precipitating in the solid state (Figures S17, S19), the spectra of the reaction solutions that led to the formation of compounds **1**, **2**, and **5** proved to be more complex; there are similarities in the relative energy of the observed bands, but there are no distinguishable features consistent between the solution and solid-state data that can serve as fingerprints to identify the solution species as has been done for the hexanuclear units.[3f,g,j, 5b, 8a, 16c, 27] It is worth noting that the intense charge-transfer band that is present in the solid-state optical spectrum of **5** is notably absent from that collected for the solution. Based on this, it is unlikely that the U_{38} cluster exists to an appreciable extent in solution, but rather only smaller polynuclear species are present.[3h,j, 17, 18] Taken together, these data highlight the complexity of U^{IV} absorbance bands given changes in solvent, coordination modes, and differences in nuclearity, whereby supplemental techniques like EXAFS and high-energy X-ray scattering techniques are useful for connecting solution speciation with observations in the solid-state.

Thermal behavior

Limited reports have focused on the thermal stability of U^{IV}-ligand complexes and clusters and, as such, the thermal behavior of **1**–**4** were examined over 25–600 °C under flowing nitrogen.[3g, 8a, 18] All compounds were found to thermally decompose over several steps (Figures S27–S30 in Supporting Information), with slight differences observed in the onset temperature, as well as the proposed decomposition products. The total weight loss observed for **1** (52.2%), **3** (53.2%) and **4** (45.8%) were consistent with thermal decomposition of the compounds to UO_2 (calculated 52.4%, 53.2%, and 47.5% for **1**, **3**, and **4**, respectively). For **4**, it is worth noting that there is approximately a 2% discrepancy in the calculated and observed weight losses assuming the formation of UO_2. By comparison, thermal decomposition of **4** to form α-U_3O_8 results in a calculated weight loss of 45.4%, which is consistent with the observed data. Hence, we cannot rule out the possibility that thermal decomposition of **4** results in the formation of α-U_3O_8. Alternatively, the total weight loss for **2** (40.3%) was consistent with thermal decomposition of the compound to $UOCl_2$ (calculated 39.2%). Interestingly, despite the observed differences in the thermal decomposition onset temperatures, number of steps, and resulting products, powder X-ray diffraction data collected at room temperature on the thermal decomposition products indexed to α-U_3O_8 (Figure S10). It is well known that UO_2 can form α-U_3O_8 under oxidizing conditions.[28] Here we attribute the observation of α-U_3O_8 to oxidation that occurs after thermogravimetric analysis, with the formation of oxidized products occurring upon cooling under air from 600 °C to room temperature. Overall these results are consistent with our previous work on An^{IV}-hydroxybenzoate clusters, which were likewise found to thermally decompose to UO_2 under flowing nitrogen.[8a] By comparison, other examinations of the thermal stability of $U_6(OH)_4O_4$ hexamers, similar to those observed in **3** and **4**, have shown these phases thermally decompose to α-U_3O_8.[29] Differences in the observed thermal decomposition products (UO_2 versus α-U_3O_8) are attributed to the conditions over which the experiment is conducted, with UO_2 forming under a nitrogen atmosphere and α-U_3O_8 forming under air.

Conclusions

The effects of synthetic conditions on U^{IV} phase formation in 2-furoate ligand systems were explored. Investigation of the solvent system (THF/H_2O), metal/ligand ratios, and temperature yielded five novel phases. The compounds were characterized by single-crystal X-ray diffraction and the structures consist of ligand bridged U^{IV} chains (**1**) or polyoxo U^{IV} clusters ranging in nuclearity from tetrameric species (**2**) to hexanuclear clusters (**3**, **4**), and ultimately nanometer sized U_{38} clusters (**5**). At relatively low water concentrations, tetrameric units were observed and with increasing ligand concentrations, ligand bridged mononuclear units were isolated. Increasing the amount of water in the reaction system pushed towards hexanuclear moieties, with two phases consisting of three distinct hexanuclear $U_6(OH)_4O_4$ cores having been characterized. Aging of the reaction from which the tetrameric clusters were isolated resulted in the formation of the U_{38} cluster but inspection of the structural chemistry of the U_4 and U_{38} clusters reveals no obvious relationship between the two oligomers. Further, the optical, magnetic, and thermal behavior of the compounds were examined. Both the magnetic and optical data are consistent with tetravalent uranium, and the UV/Vis absorption spectra of **1**–**5** highlight the rich spectroscopic signatures characteristic of U^{IV}, which are influenced by coordination number, metal environment, and solvent. Collectively, the results points to the rich structural chemistry of U^{IV} that arises from hydrolysis and condensation, ligand complexation, and the influences thereon of synthetic conditions.

Experimental Section

Materials

2-Furoic acid (98%, ACROS) was used as received and UCl_4 was synthesized following published literature procedures.[8a,30] Nanopure water (≤0.05 μS; Millipore USA) and tetrahydrofuran (>99%, Fisher) were used in the syntheses that follow. To prevent oxidation of U^{IV}, nanopure water was boiled and degassed, and tetrahydrofuran was dried and stored over 4 Å sieves in a N_2 atmosphere. A nitrogen glove box was used for all synthetic manipulations.

Synthesis

Caution: ^{238}U is an alpha-emitting radionuclide and standard precautions for handling radioactive material should be followed when working with the quantities used in the syntheses that follow.

For compounds **1**–**4**, the syntheses detailed below are for those reactions with the M:L ratio that corresponds to the stoichiometry observed in the crystalline material. The formation of the phases (and yield) was further explored as a function of metal/ligand ratio using nearly identical synthetic parameters (e.g., reaction time and temperature), with the exception of the concentration of the metal salt or organic ligand.

$[UCl_2(2\text{-}FA)_2(H_2O)_2]_n$ (1): 2-Furoic acid (0.34 g, 3.0 mmol) was dissolved into a solution of UCl_4 (0.075 g, 0.20 mmol) in THF (1.77 g, 24.5 mmol) and H_2O (0.010 g, 0.56 mmol) in a 15 mL thick walled pressure tube. The pressure tube was sealed and heated at 50 °C in a heating block. After five days, green rectangular crystals deposited at the bottom of the tube. The crystals were separated from a clear, green solution and left to dry under N_2. Yield based on U: 0.078 g, 70%; elemental analysis (%); calc (found): C: 21.50 (21.18); H: 1.83 (1.78); N: 0.0 (0.0).

$[U_4Cl_{10}O_2(THF)_6(2\text{-}FA)_2]\cdot 2\,THF$ (2): UCl_4 (0.075 g, 0.20 mmol) was dissolved into THF (1.77 g, 24.5 mmol). The solution was transferred to a 15 mL thick walled pressure tube containing 2-furoic acid (0.011 g, 0.10 mmol). An aliquot of water (0.010 g, 0.56 mmol) was added. The tube was then sealed and heated at 50 °C in a heating block. After one week, small green block crystals deposited at the bottom of the tube. The crystals were separated from a clear dark green mother liquor and left to dry under N_2. Yield based on U: 0.054 g, 46%; elemental analysis (%); calc (found): C: 23.22 (23.60); H: 3.26(3.30); N: 0.0 (0.0).

$[U_6O_4(OH)_4(H_2O)_3(2\text{-}FA)_{12}]\cdot 7\,THF\cdot H_2O$ (3): 2-Furoic acid (0.045 g, 0.40 mmol) was dissolved into THF (0.445 g, 6.16 mmol) in a 15 mL thick walled pressure tube. In a separate vial, UCl_4 (0.075 g, 0.20 mmol) was dissolved into H_2O (1.50 g, 83.1 mmol). The UCl_4 solution was then added to the pressure tube. The tube was sealed and placed in a heating block set at 50 °C. After 24 hours, green square crystals deposited on the bottom of the tube. After 48 hours, crystals were harvested from a clear, green solution and left to dry under N_2. Yield based on U: 0.042 g, 37%: elemental analysis (%); calc (found): C: 30.46 (30.27); H: 3.02 (3.07); N: 0.0 (0.0).

$[U_6O_4(OH)_4(H_2O)_2(2\text{-}FA)_{12}]\cdot 8.76\,H_2O$ (4): UCl_4 (0.075 g, 0.20 mmol) was dissolved into H_2O (2.0 g, 111 mmol). The solution was then transferred to a 15 mL thick walled pressure tube containing 2-furoic acid (0.045 g, 0.40 mmol). The ligand did not completely dissolve upon addition of the aqueous U solution and a white solid was present at the bottom of the reaction vessel. The pressure tube was then closed and set in a heating block at 50 °C. After 24 hours, green needle-like crystals formed; the white precipitate was no longer observed. The crystals were separated from a clear, green solution after 48 hours and dried under N_2. Yield based on U: 0.060 g, 60%; elemental analysis (%); calc (found): C: 23.44 (23.33); H: 2.00 (2.05); N: 0.0 (0.0).

$[U_{38}Cl_{42}O_{56}(H_2O)_{20}]\cdot m\,H_2O\cdot n\,THF$ (5): A solution of UCl_4 (0.075 g, 0.20 mmol) in THF (1.77 g, 24.5 mmol) was transferred to a 6 mL screw capped vial containing 2-furoic acid (0.045 g, 0.40 mmol). An aliquot of H_2O (0.010 g, 0.56 mmol) was added. The vial was capped and placed in a heating block set to 50 °C. After one week, crystals of **1** were observed in varying yield; however, prolonged heating of the reaction (approximately five months) resulted in the formation of small reddish-orange block crystals and a green precipitate. The reaction was reproduced several times to ensure reproducibility of **5** and it is worth noting that loss of solvent led to the formation of **2**. Crystals of **5** were separated from a clear, dark green solution and left to dry under N_2. Approximate yield based on U: 0.018 g, 29%. Instability of the crystals precluded the elemental analysis, powder X-ray diffraction characterization, and thermal gravimetric analysis of **5**.

X-Ray structure determination: Single crystals of each compound were selected from the bulk and mounted in paratone oil on a MiTeGen micromount. Data for compounds **1**–**5** were collected on a Bruker D8 Quest equipped with a $Mo_{K\alpha}$ radiation source (λ = 0.71073 Å) and a Photon100 CMOS detector at 100 K. Data were collected using a combination of phi and omega scans and integrated with the Bruker SAINT program.[31] Intensities were corrected for Lorentz and polarization effects and an empirical absorption correction was applied using SADABS (TWINABS v2012 for **4**).[31,32] Structure solutions were performed using the SHELXTL software suite.[31] Non-hydrogen atoms were refined with anisotropic thermal parameters and hydrogen atoms were included in idealized positions unless otherwise noted. Crystallographic information for compounds **1**–**5** is provided in Table 1. Further details of the structure refinement of **1**–**5**, including modeling of disordered portions of the ligands, are available in the Supporting Information.

CCDC 1916309, 1916310, 1916311, 1916312, and 1916313 contain the supplementary crystallographic data for this paper. These data are provided free of charge by The Cambridge Crystallographic Data Centre.

Powder X-ray diffraction: Powder X-ray diffraction (PXRD) data were collected for compounds **1**–**4** using a Rigaku Ultima IV diffractometer ($Cu_{K\alpha}$ λ = 1.542 Å, 2θ = 3–40°). Agreement between the calculated and observed patterns (Figures S6–S9) supported that the single crystals used for structure determination were representative of the bulk sample. The limited yield of **5** and instability of the crystals precluded bulk analysis. PXRD data were also collected on the thermal decomposition products of **1**–**4** (see below) and were consistent with U_3O_8 (ICSD reference code 24906; Figure S10). UO_2 nanoparticles resulting from the temperature studies (see below) were confirmed through comparison of the experimental powder pattern with that reported for UO_2 (ICSD reference code 29086; Figures S11–S14).

Elemental analysis: Combustion elemental analysis (EA) was collected on a PerkinElmer Model 2400 Elemental Analyzer. Samples of **1**–**4** (1.5–2.0 mg) were weighed into small tin capsules. The samples were run in triplicate and the reported value is the average.

UO_2 nanoparticle preparation: A synthetic procedure similar to that described above for **1**–**4** was used to study the effects of temperature on UO_2 nanoparticle formation. The reaction solutions from which **1**–**3** crystallized were heated for an hour at 100 °C while **4** was heated at 120 °C. The solution from which **4** crystallized was heated at 120 °C as UO_2 nanoparticles were not observed

Table 1. Crystallographic Structure Refinement Details for 1–5 (100 K).[a]

	1	2	3	4	5
formula	$UC1_2O_8C_{10}H_{10}$	$U_4Cl_{10}O_{16}C_{42}H_{70}$	$U_6O_{55}C_{88}H_{104}$	$U_6O_{54.76}C_{60}H_{61.52}$	$U_{38}Cl_{42}O_{76}H_{42}$
M_W [g mol^{-1}]	567.11	2137.60	3469.89	3087.03	11792.37
temperature [K]	100(2)	100(2)	100(2)	100(2)	100(2)
crystal system	monoclinic	monoclinic	trigonal	triclinic	tetragonal
space group	*C2/c*	$P2_1/n$	$P3_1c$	$P\bar{1}$	*I4/m*
λ [Å]	0.71073	0.71073	0.71073	0.71073	0.71073
a [Å]	21.5967(11)	11.8122(8)	17.1078(7)	13.6331(9)	21.0554(14)
b [Å]	6.6177(4)	13.8381(9)	17.1078(7)	14.3408(9)	21.0554(14)
c [Å]	10.3121(5)	18.4492(12)	21.5601(10)	20.6797(14)	27.741(2)
α [°]	90	90	90	85.026(2)	90
β [°]	110.122(2)	98.1420(19)	90	84.864(2)	90
γ [°]	90	90	120	79.214(2)	90
volume [Å^3]	1383.85(13)	2985.3(3)	5464.7(5)	3945.6(4)	12298.5(19)
Z	4	2	2	2	2
ρ [g cm^{-3}]	2.703	2.378	2.101	2.577	3.173
μ [mm^{-1}]	12.150	11.324	8.954	12.383	25.407
R_1	0.0139	0.0194	0.0570	0.0707	0.0635
wR_2	0.0307	0.0435	0.1382	0.1205	0.2161
GOF	1.089	1.040	1.238	1.023	1.054
CCDC	1916310	1916309	1916311	1916312	1916313

[a] The formula and formula weight reported for **5** excludes solvent molecules in the outer coordination sphere as these were not located during refinement.

below that temperature. After heating, the tube was removed from heat and allowed to cool for 1 hour. The forest green solution was then transferred to a centrifuge tube and 5 mL EtOH was added. The diluted solution was centrifuged for 10 minutes at 4500 rpm, resulting in the formation of two layers, a clear layer and a dark green layer. The clear layer was disposed, and the dark green solution was washed and centrifuged another two times. After the final cycle, the dark green solution, containing the UO_2 nanoparticles, was then drop-cast onto a sample holder for analysis by powder X-ray diffraction. TEM samples were prepared by dipping carbon-coated copper grids into a solution of 10 μL of the UO_2 nanoparticle solution and 5 mL of a mixture of THF/H_2O dependent upon the ratio used in the synthetic procedure. The grids were then left to dry under ambient conditions for 24 hours before TEM measurements were collected.

High-resolution transmission electron microscopy (HRTEM): Solutions were prepared following the procedure that yielded **1**–**4** and subsequently heated to 100–120 °C. Particle imaging was performed on a JEOL JEM-2100F FEG-TEM operated at 200 kV at the Advanced Imaging and Microscopy Lab at the University of Maryland. Samples were prepared by dipping carbon-coated copper grids in dilute nanomaterial solutions and drying at room temperature. Fourier transform measurements of the images were performed using ImageJ software to generate diffraction spots for determining distances between atomic planes (Figures S61–S68).

Infrared and Raman spectroscopy: Infrared spectra of **1**–**5** were collected on a Perkin–Elmer FTIR Spectrum 2 system (Figure S22–S26). The samples were collected using a diamond ATR-FTIR attachment. Data were collected over 400–4000 cm^{-1} with 16 scans and 2 cm^{-1} resolution. The data were acquired using the Spectrum Quant software program. Raman spectra of single crystals of **1**–**4** were collected on a HORIBA LabRAM HR Evolution Raman Microscope over 150–3500 cm^{-1} with an excitation line of 532 nm at 40 accumulations and an acquisition time of 6 seconds (Figure S22–S25). We note that the crystals of **5** were unstable and no matter the laser power the crystals decomposed during attempted Raman collections, therefore, only the IR spectrum is presented for **5** (Figure S26).

UV-Vis-NIR spectroscopy: Optical spectra for **1**–**4** were collected on an Agilent Technologies Cary 5000 UV/Vis-NIR using a diffuse reflectance attachment. The solid sample (20.0 mg) was mixed with polymethylmethacrylate (0.100 g) to give a uniform sample coverage in the solid-state sample holder. The spectra were collected from 400 to 700 nm with a scan rate of 600 nm min^{-1} using the Cary WinUV program. The UV/Vis-NIR spectrum for **5** was collected using a CRAIC 20/30 PV Technologies microspectrophotometer. Single crystals of **5** were placed on a quartz slide in oil and data was collected from 320–1700 nm (Figure 11). Optical spectra for the solutions from which **1**–**5** crystallized were collected on an Agilent Technologies Cary 5000 UV/Vis-NIR with a double beam liquid attachment using the Cary WinUV program in quartz cuvettes. The spectra were collected from 400 to 700 nm with a scan rate of 600 nm min^{-1}. The mother liquor was collected just prior to crystallization and samples were prepared through dilution of 1 mL of the mother liquor into 3 mL of the appropriate solvent system (Figure S15–S17, S19, S20).

Magnetic studies: Magnetic susceptibility data for **1**–**5** were collected using a Quantum Design MPMS-7 SQUID magnetometer. Samples were prepared in a dinitrogen filled glovebox (Vacuum Atmospheres, Inc. Nexus II) under inert conditions. Powdered samples were loaded into polyethylene bags and the bags were subsequently sealed using a Ziploc v159 Vacuum Sealer System. The bags were then removed from the glovebox and folded and inserted into a plastic drinking straw. Ferromagnetic impurities were checked through variable field analyses (0 to 20 kOe) of magnetization at 100 K (Figures S31–S35). Saturation of magnetization measurements were performed at 2 K varying the applied field up to 70 kOe (Figures S36–S40). Magnetic susceptibility data were collected at temperatures ranging from 2 to 300 K (Figure S41–S60). For compounds **1** and **2** applied fields of 1000 Oe were used, whereas for **3** and **4** applied fields of 5000 Oe were used and finally for **5**, an applied field of 10000 Oe was used. Reproducibility of the magnetic susceptibility data was checked over two separate

batches for each compound measured (Figures S43, S47, S51 and S55) expect for **5**. Data were corrected for the diamagnetic contributions of the sample holder and bag by subtracting empty containers; corrections for the sample were calculated from Pascal's constants.[33]

Thermogravimetric Analysis: Thermogravimetric analysis data were collected on a TA instruments Q50 system Thermogravimetric Analyzer. Samples of **1** (10.4690 mg), **2** (11.3750 mg), **3** (15.1300 mg), and **4** (10.6450 mg) were weighed out into platinum pans. The temperature was held at 25 °C for 5 minutes to dry off excess water after which the samples were heated to 600 °C at 5 °C min^{-1} under flowing nitrogen (10 mL min^{-1}). For **3**, the outer coordination solvent molecules were driven off when the sample was heated to 100 °C at 5 °C min^{-1} under flowing nitrogen (10 mL min^{-1}) and held at 100 °C for 60 minutes before the sample was heated to 600 °C. The software TA universal analysis was used to collect and process the data (Figure S27–S30).

Funding Sources

U.S. Department of Energy, Office of Science, Office of Basic Energy Sciences, Early Career Research Program under Award DE-SC0019190; National Science Foundation for acquisition of the Raman spectrometer and single crystal X-ray diffractometer under grants NSF CHE-1429079 and NSF CHE-1337975, respectively. The Nature Conservancy; U.S. Department of Energy, Office of Science, Basic Energy Sciences, under the Separations Science program (DE-SC0017259); U.S. Department of Energy, Office of Science, Office of Basic Energy Sciences, Heavy Elements Chemistry Program under Award Number DE-FG02-13ER16414; U.S. Department of Energy, Office of Science, Office of Workforce Development for Teachers and Scientists, Office of Science Graduate Student Research (SCGSR) program.

Acknowledgements

The primary source of support for this work is the U.S. Department of Energy, Office of Science, Office of Basic Energy Sciences, Early Career Research Program under Award DE-SC0019190. The syntheses, structural analysis, and characterization of the U phases were performed at Georgetown University by N.A.V. and K.E.K., supported under this award. The authors also thank the National Science Foundation under grants NSF CHE-1337975 and NSF CHE-1429079 for SCXRD and Raman instrumentation, respectively. R.F.H. and E.J.S. collected magnetic data for compounds **1**–**5**. R.F.H. and E.J.S. thank the NatureNet Science Fellowship program from The Nature Conservancy for support. E.J.S. also thanks the U.S. Department of Energy, Office of Science, Basic Energy Sciences, Separations and Analysis program under Award Number DE-SC0017259 for financial support. D.R.C.A. and S.L.S. collected the TEM images and helped with data interpretation and are supported by NSF-NSF (CHE-1904616) and NSF (CHE-1607905). E.W. collected UV/Vis-NIR spectra for **5**; J.N.W. and S.A.K. provided supporting UV/Vis-NIR data for this compound. E.W. is supported by the U.S. Department of Energy, Office of Science, Office of Basic Energy Sciences, Heavy Elements Chemistry Program under Award Number DE-FG02-13ER16414. J.N.W. was supported in part by the U.S. Department of Energy, Office of Science, Office of Workforce Development for Teachers and Scientists, Office of Science Graduate Student Research (SCGSR) program. The SCGSR program is administered by the Oak Ridge Institute for Science and Education (ORISE) for the DOE. ORISE is managed by ORAU under contract number DE-SC0014664. S.A.K. is supported by the Department of Energy, Office of Science, Office of Basic Energy Sciences, Heavy Element Chemistry Program. Los Alamos National Laboratory is an affirmative action/equal opportunity employer, managed by Triad National Security, LLC, for the NNSA of the U.S. Department of Energy (contract 89233218CNA000001).

Conflict of interest

The authors declare no conflict of interest.

Keywords: 2-furoic acid · crystallization · hydrolysis · uranium · X-ray diffraction

[1] a) C. F. Baes, R. E. Mesmer, *The Hydrolysis of Cations*, Wiley, New York, **1976**; b) P. L. Brown, C. Ekberg, *Hydrolysis of Metal Ions*, Wiley-VCH, Weinheim, **2016**; c) M. Henry, J. P. Jolivet, L. Livage in *Structure and Bonding*, Springer, Berlin, **1992**, p. 155.

[2] a) A. Novikov, S. N. Kalmykov, S. Utsunomiya, R. C. Ewing, F. Horreard, A. Merkulov, S. B. Clark, V. V. Tkachev, B. F. Myasoedov, *Science* **2006**, *314*, 638–641; b) R. J. Silva, H. Nitsche, *Radiochim. Acta* **1995**, *70–71*, 377–396.

[3] a) G. E. Sigmon, A. E. Hixon, *Chem. Eur. J.* **2019**, *25*, 2463–2466; b) Y.-J. Hu, K. E. Knope, S. Skanthakumar, L. Soderholm, *Eur. J. Inorg. Chem.* **2013**, 4159–4163; c) K. E. Knope, L. Soderholm, *Chem. Rev.* **2013**, *113*, 944–994; d) L. Soderholm, P. M. Almond, S. Skanthakumar, R. E. Wilson, P. C. Burns, *Angew. Chem. Int. Ed.* **2008**, *47*, 298–302; *Angew. Chem.* **2008**, *120*, 304–308; e) R. E. Wilson, S. Skanthakumar, L. Soderholm, *Angew. Chem. Int. Ed.* **2011**, *50*, 11234–11237; *Angew. Chem.* **2011**, *123*, 11430–11433; f) C. Falaise, H. A. Neal, M. Nyman, *Inorg. Chem.* **2017**, *56*, 6591–6598; g) C. Falaise, C. Volkringer, T. Loiseau, *Cryst. Growth Des.* **2013**, *13*, 3225–3231; h) C. Falaise, C. Volkringer, J.-F. Vigier, A. Beaurain, P. Roussel, P. Rabu, T. Loiseau, *J. Am. Chem. Soc.* **2013**, *135*, 15678–15681; i) C. Falaise, C. Volkringer, J.-F. Vigier, N. Henry, A. Beaurain, T. Loiseau, *Chem. Eur. J.* **2013**, *19*, 5324–5331; j) L. Chatelain, R. Faizova, F. Fadaei-Tirani, J. Pecaut, M. Mazzanti, *Angew. Chem. Int. Ed.* **2019**, *58*, 3021–3026; *Angew. Chem.* **2019**, *131*, 3053–3058.

[4] N. P. Martin, C. Volkringer, P. Roussel, J. Marz, C. Hennig, T. Loiseau, A. Ikeda-Ohno, *Chem. Commun.* **2018**, *54*, 10060–10063.

[5] a) P. Li, X. Wang, K.-i. Otake, J. Lyu, S. L. Hanna, T. Islamoglu, O. K. Farha, *ACS Appl. Nano Mater.* **2019**, *2*, 2260–2265; b) C. Tamain, T. Dumas, C. Hennig, P. Guilbaud, *Chem. Eur. J.* **2017**, *23*, 6864–6875.

[6] P. Li, S. Goswami, K.-i. Otake, X. Wang, Z. Chen, S. L. Hanna, O. K. Farha, *Inorg. Chem.* **2019**, *58*, 3586–3590.

[7] S. E. Gilson, P. Li, J. E. S. Szymanowski, J. White, D. Ray, L. Gagliardi, O. K. Farha, P. C. Burns, *J. Am. Chem. Soc.* **2019**, *141*, 11842–11846.

[8] a) N. A. Vanagas, J. N. Wacker, C. L. Rom, E. N. Glass, I. Colliard, Y. Qiao, J. A. Bertke, E. Van Keuren, E. J. Schelter, M. Nyman, K. E. Knope, *Inorg. Chem.* **2018**, *57*, 7259–7269; b) J. N. Wacker, S. Y. Han, A. V. Murray, N. A. Vanagas, J. A. Bertke, J. M. Sperling, R. G. Surbella, K. E. Knope, *Inorg. Chem.* **2019**, *58*, 10578–10591; c) J. N. Wacker, M. Vasiliu, I. Colliard, R. L. Ayscue, S. Y. Han, J. A. Bertke, M. Nyman, D. A. Dixon, K. E. Knope, *Inorg. Chem.* **2019**, *58*, 10871–10882; d) J. N. Wacker, M. Vasiliu, K. Huang, R. E. Baumbach, J. A. Bertke, D. A. Dixon, K. E. Knope, *Inorg. Chem.* **2017**, *56*, 9772–9780.

[9] a) A. K. Cheetham, G. Kieslich, H. H. M. Yeung, *Acc. Chem. Res.* **2018**, *51*, 659–667; b) P. M. Forster, A. R. Burbank, C. Livage, G. Férey, A. K. Cheetham, *Chem. Commun.* **2004**, 368–369; c) P. M. Forster, N. Stock, A. K. Cheetham, *Angew. Chem. Int. Ed.* **2005**, *44*, 7608–7611; *Angew. Chem.* **2005**, *117*, 7780–7784.

[10] C. Hennig, S. Takao, K. Takao, S. Weiss, W. Kraus, F. Emmerling, A. C. Scheinost, *Dalton Trans.* **2012**, *41*, 12818 – 12823.
[11] C. Falaise, C. Volkringer, T. Loiseau, *Inorg. Chem. Commun.* **2014**, *39*, 26 – 30.
[12] a) I. Jelenić, D. Grdenić, A. Bezjak, *Acta Crystallogr.* **1964**, *17*, 758 – 759; b) D. Grdenić, B. Korpar-Colig, *J. Inorg. Nucl. Chem.* **1968**, *30*, 1751 – 1755.
[13] C. R. Groom, I. J. Bruno, M. P. Lightfoot, S. C. Ward, *Acta Crystallogr. Sect. B* **2016**, *72*, 171 – 179.
[14] a) A. J. Gaunt, B. L. Scott, M. P. Neu, *Inorg. Chem.* **2006**, *45*, 7401 – 7407; b) J. D. Rinehart, S. A. Kozimor, J. R. Long, *Angew. Chem. Int. Ed.* **2010**, *49*, 2560 – 2564; *Angew. Chem.* **2010**, *122*, 2614 – 2618; c) J. G. Reynolds, A. Zalkin, D. H. Templeton, N. M. Edelstein, *Inorg. Chem.* **1977**, *16*, 1858 – 1861; d) J. C. Berthet, P. Thuéry, M. Ephritikhine, *Eur. J. Inorg. Chem.* **2008**, 5455 – 5459; e) N. Brianese, U. Castellato, F. Ossola, M. Porchia, G. Rossetto, P. Zanella, R. Graziani, *J. Organomet. Chem.* **1989**, *365*, 223 – 232; f) J. C. Berthet, P. Thuery, M. Ephritikhine, *CSD Communication*, **2013**; g) F. Calderazzo, G. Dell′ Amico, M. Pasquali, G. Perego, *Inorg. Chem.* **1978**, *17*, 474 – 479; h) A. Domingos, N. Marques, A. Pires do Matos, I. Santos, M. Silva, *Polyhedron* **1992**, *11*, 2021 – 2025.
[15] L. Salmon, P. Thuéry, M. Ephritikhine, *Polyhedron* **2006**, *25*, 1537 – 1542.
[16] a) G. Lundgren, *Ark. Kemi* **1953**, *5*, 349; b) J.-C. Berthet, P. Thuéry, M. Ephritikhine, *Chem. Commun.* **2005**, 3415 – 3417; c) L. M. Mokry, N. S. Dean, C. J. Carrano, *Angew. Chem. Int. Ed. Engl.* **1996**, *35*, 1497 – 1498; *Angew. Chem.* **1996**, *108*, 1676 – 1677; d) G. Nocton, J. Pécaut, Y. Filinchuk, M. Mazzanti, *Chem. Commun.* **2010**, *46*, 2757 – 2759; e) S. Takao, K. Takao, W. Kraus, F. Emmerling, A. C. Scheinost, G. Bernhard, C. Hennig, *Eur. J. Inorg. Chem.* **2009**, 4771 – 4775; f) K. E. Knope, L. Soderholm, *Inorg. Chem.* **2013**, *52*, 6770 – 6772; g) K. E. Knope, R. E. Wilson, M. Vasiliu, D. A. Dixon, L. Soderholm, *Inorg. Chem.* **2011**, *50*, 9696 – 9704; h) K. Takao, S. Takao, A. C. Scheinost, G. Bernhard, C. Hennig, *Inorg. Chem.* **2012**, *51*, 1336 – 1344.
[17] a) B. Biswas, V. Mougel, J. Pécaut, M. Mazzanti, *Angew. Chem. Int. Ed.* **2011**, *50*, 5745 – 5748; *Angew. Chem.* **2011**, *123*, 5863 – 5866; b) G. Nocton, F. Burdet, J. Pécaut, M. Mazzanti, *Angew. Chem. Int. Ed.* **2007**, *46*, 7574 – 7578; *Angew. Chem.* **2007**, *119*, 7718 – 7722.
[18] N. P. Martin, C. Volkringer, N. Henry, X. Trivelli, G. Stoclet, A. Ikeda-Ohno, T. Loiseau, *Chem. Sci.* **2018**, *9*, 5021 – 5032.
[19] N. E. Brese, M. O'Keeffe, *Acta Crystallogr. Sect. B* **1991**, *47*, 192 – 197.
[20] M. Dufaye, N. P. Martin, S. Duval, C. Volkringer, A. Ikeda-Ohno, T. Loiseau, *RSC Adv.* **2019**, *9*, 22795 – 22804.
[21] J. K. Gibson, R. G. Haire, *J. Alloys Compd.* **2001**, *322*, 143 – 152.
[22] D. R. Kindra, W. J. Evans, *Chem. Rev.* **2014**, *114*, 8865 – 8882.
[23] K. R. Meihaus, J. R. Long, *Dalton Trans.* **2015**, *44*, 2517 – 2528.
[24] a) P. L. Arnold, G. M. Jones, S. O. Odoh, G. Schreckenbach, N. Magnani, J. B. Love, *Nat. Chem.* **2012**, *4*, 221 – 227; b) G. Nocton, P. Horeglad, J. Pecaut, M. Mazzanti, *J. Am. Chem. Soc.* **2008**, *130*, 16633 – 16645; c) P. B. Duval, C. J. Burns, D. L. Clark, D. E. Morris, B. L. Scott, J. D. Thompson, E. L. Werkema, L. Jia, R. A. Andersen, *Angew. Chem. Int. Ed.* **2001**, *40*, 3357 – 3361; *Angew. Chem.* **2001**, *113*, 3461 – 3465.
[25] C. Falaise, J. Delille, C. Volkringer, T. Loiseau, *Eur. J. Inorg. Chem.* **2015**, 2813 – 2821.
[26] a) J. G. Conway, *J. Chem. Phys.* **1959**, *31*, 1002 – 1004; b) W. T. Carnall, G. K. Liu, C. W. Williams, M. F. Reid, *J. Chem. Phys.* **1991**, *95*, 7194 – 7203.
[27] a) J. Ling, H. Lu, Y. Wang, K. Johnson, S. Wang, *RSC Adv.* **2018**, *8*, 34947 – 34953; b) J. Diwu, J. J. Good, V. H. DiStefano, T. E. Albrecht-Schmitt, *Eur. J. Inorg. Chem.* **2011**, 1374 – 1377.
[28] a) K. O. Kvashnina, S. M. Butorin, P. Martin, P. Glatzel, *Phys. Rev. Lett.* **2013**, *111*, 253002; b) R. J. McEachern, P. Taylor, *J. Nucl. Mater.* **1998**, *254*, 87 – 121; c) G. Rousseau, L. Desgranges, F. Charlot, N. Millot, J. C. Nièpce, M. Pijolat, F. Valdivieso, G. Baldinozzi, J. F. Bérar, *J. Nucl. Mater.* **2006**, *355*, 10 – 20.
[29] I. Grenthe, J. Drozydzyn, T. Fujino, E. C. Buck, T. E. Albrecht-Schmitt, S. F. Wolf in *The Chemistry of the Actinide and Transactinide Elements*, 4th ed. (Eds.: L. R. Morss, N. M. Edelstein, J. Fuger), Springer, Dordrecht, **2010**, pp. 253 – 698.
[30] J. L. Kiplinger, D. E. Morris, B. L. Scott, C. J. Burns, *Organometallics* **2002**, *21*, 5978 – 5982.
[31] Bruker, Bruker AXS, Inc., Madison, Wisconsin, USA, **2014**.
[32] Bruker, Vol. 2012/1, Bruker AXS Inc., Madison, Wisconsin, USA, **2001**.
[33] G. A. Bain, J. F. Berry, *J. Chem. Educ.* **2008**, *85*, 532 – 536.

Manuscript received: December 21, 2019
Accepted manuscript online: January 30, 2020
Version of record online: April 21, 2020